Check for updates

physica status solidi b

www.pss-b.com

Janus Monolayers of Transition Metal Dichalcogenides: A DFT Study

*Miguel Ángel Hernández-Vázquez, Andrés de Luna Bugallo, and Daniel Olguín**

A computational study is presented using a sequence of full-potential linearized augmented plane-wave method (FP-LAPW) within the generalized gradient approximation as well as the on-site hybrid functionals for the exchange–correlation energy to determine the structural and electronic properties of Janus transition metal dichalcogenide monolayers in MoXY (X, Y = S, Se, Te with X different from Y) configurations. The calculated electronic band structures of the studied Janus monolayers show a Rashba splitting around the Γ point and the Zeeman spin-splitting at the K_- and K_+ points. The findings suggest that these materials represent interesting 2D systems to develop different applications such as orbitronics.

1. Introduction

An atomically thin monolayer of transition metal dichalcogenides (TMDs) is highly asymmetric along the *c*-axis. This asymmetry induces a strong spin–orbit coupling (SOC), giving rise to interesting physical phenomena such as spin–valley locking and light–matter enhancement that can be implemented in valleytronics and spintronics.[1–3] Recent works have demonstrated that MXY (M = W, Mo; X, Y = S, Se, Te, with X different from Y at the same time) Janus monolayers are also noncentrosymmetric systems resulting in strong SOC effects.[4,5] In addition, if X and Y correspond to the same atoms, TMD single layers are direct bandgap semiconductors.[6] However, suppose X and Y belong to different chalcogen atoms, the Janus monolayer becomes an indirect semiconductor where the Rashba spin-splitting occurs at the valence band maximum (VBM) around Γ point.[7,8]

In this work, by using the full-potential linearized augmented plane-wave method (FP-LAPW), we study the electronic properties of the Mo-XY (X = S, Se, Te) monolayers. We show that Janus monolayer with X = S and Y = Se allows manipulating the Rashba effect so that the system can be proposed as valleytronic and spintronic systems. The paper is organized as follows; Section 2 shows the generalities of the used method, our results are discussed in Section 3, a final Section 4 shows our conclusions.

2. Method

FP-LAPW implemented in the WIEN2K code was used for our computational calculations.[9] In this method, wave functions, charge density, and potential are expanded in spherical harmonics within nonoverlapping muffin-tin spheres and plane waves used in the remaining interstitial region of the unit cell. In the code, the core and valence states are treated differently. Core states are treated within a multiconfiguration relativistic Dirac–Fock approach, while valence states are treated in a scalar relativistic approach. The exchange–correlation energy was calculated using the generalized gradient approximation (GGA) correction of Perdew et al.[10] and the on-site hybrid functional implemented in the Wien2k code.[11–13] We studied the Mo-XY (X, Y = S, Se, Te) monolayer system using the slab model (**Figure 1**). To properly isolate each slab from their periodic images and to avoid large vacuum zones, which, in plane wave methods, considerably increase the demand of computational resources, a vacuum of 10.5 Å with the upper slab was considered for the layered systems. The atomic electronic configuration used in our calculations was Mo: [Kr] $4d^5\ 5s^1$; Te: [Kr] $4d^{10}\ 5s^2\ 5p^4$; S: [Ne] $3s^2\ 3p^4$; and Se: [Ar] $3d^{10}\ 4s^2\ 4p^4$.

Precise step analysis was done to ensure convergence of the total energy in terms of the variational parameters, the muffin-thin radius (MTR), and the cutoff energy (G_{Max}), where the values used for the MoTeSe system: $MTR_{Mo} = 2.37$, $MTR_{Se} = 2.37$, $MTR_{Te} = 2.5$, $G_{Max} = 12.5\ bohr^{-1}$, for the MoTeS system: $MTR_{Mo} = 2.42$, $MTR_{Te} = 2.08$, $MTR_S = 2.5$, $G_{Max} = 13\ bohr^{-1}$, and for the MoSSe system: $MTR_{Mo} = 2.35$, $MTR_S = 2.10$, $MTR_{Se} = 2.39$, $G_{Max} = 12\ bohr^{-1}$. At the same time, for the three systems studied, we have used an appropriate set of *k*-points to compute the total energy, where a set of 120 *k*-points in the

M. Á. Hernández-Vázquez
Centro de Investigación y de Estudios Avanzados del I. P. N.
Unidad Querétaro
Libramiento Norponiente No. 2000, Fracc. Real de Juriquilla, Querétaro, Qro. CP 76230, México

A. de Luna Bugallo
Centro de Física Aplicada y Tecnología Avanzada
UNAM
AP 1-1010, Querétaro, Qro. CP 76000, Mexico

D. Olguín
Departamento de Física
Centro de Investigación y de Estudios Avanzados del IPN
Av. IPN 2508, Col. San Pedro Zacatenco, Ciudad de México CP 07200, México
E-mail: daniel@fis.cinvestav.mx

The ORCID identification number(s) for the author(s) of this article can be found under https://doi.org/10.1002/pssb.202100248.

DOI: 10.1002/pssb.202100248

 © 2021 Wiley-VCH GmbH

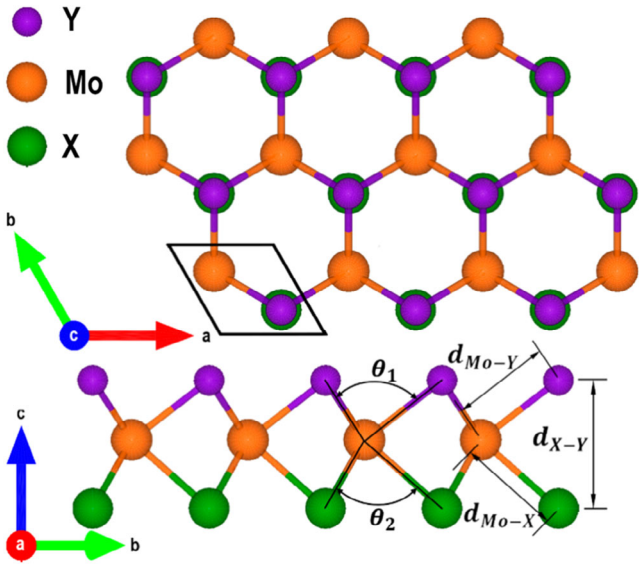

Figure 1. Schematic representation of the slab model used in our calculations, top and side view, for the Mo-XY (X, Y = S, Se, Te) system structures.

Table 1. Structural parameters for Mo-XY monolayers, distances, and angles between Mo-XY atoms as illustrated in Figure 1.

	MoSTe	MoSeTe	MoSSe
d_{Mo-X} [Å]	2.44[a]	2.56[a]	2.43[a]
	2.45[b]	2.57[b]	2.43[b]
	2.41[c]	2.52[c]	2.40[c]
d_{Mo-Y} [Å]	2.71[a]	2.72[a]	2.55[a]
	2.72[b]	2.72[b]	2.55[b]
	2.68[c]	2.68[c]	2.51[c]
d_{X-Y} [Å]	3.30[a]	3.43[a]	3.27[a]
	3.32[b]	3.44[b]	3.27[b]
	3.26[c]	3.38[c]	3.22[c]
θ_1 [°]	78.04[a),b),c)]	79.42[a),b),c)]	79.26[a),b),c)]
θ_2 [°]	88.57[a),b),c)]	85.47[a),b),c)]	83.97[a),b),c)]
a [Å]	3.41[a]	3.48[a]	3.25[a]
	3.42[b]	3.48[b]	3.25[b]
	3.37[c]	3.42[c]	3.18[c]
	3.36[d]	3.43[d]	3.25[d]

[a]GGA; [b]GGA-hybrid; [c]LDA-hybrid; [d]HSE06: ref. [5].

irreducible sector of Brillouin zone was used, equivalent to a $(19 \times 19 \times 4)$ Monkhorst–Pack grid in the unit cell.[14]

To get the stable geometry for the different substitutions studied, a fully relaxed calculation for all the atomic positions in the supercell was done, where the criterion for convergence is 0.001 Ry au^{-1}. Then, by computing the total energy of a primitive cell as a function of the volume and fitting the data with the Murnaghan relation,[15] the lattice parameters were obtained for each studied system.

3. Results and Discussion

3.1. Structural Parameters

The crystal structure of MXY monolayers is hexagonal (space group *P-6m2* when X equals Y and *P3m1* in the other case). **Table 1** shows a comparison of the structural parameters (to identify the used labels, see Figure 1) obtained in our calculations using (a) GGA, (b) GGA-hybrid, and (c) local density approximation (LDA)-hybrid with those reported in the computational database of 2D materials (see refs. [5,16,17]). As we have found, in the Janus monolayer, the nearest neighbor distances show the trend $d_{\text{Mo-SeTe}} > d_{\text{Mo-STe}} > d_{\text{MoSSe}}$, in good agreement with recent data reported in the literature.[4,18–20] The same trend is also shown for the apical distance d_{X-Y} (see Figure 1). The angle θ_1 for the X_{light}–Mo–X_{light} bonding is smaller than angle θ_2 for the Y_{heavy}–Mo–Y_{heavy}, where X_{light} (Y_{heavy}) means the light (heavy) chalcogen in the Mo-XY Janus monolayer, showing in this way a bending strain from the heavy to the light chalcogen plane.[18] Then, our calculated in-plane lattice parameter is also in good agreement with recently published data.[4] Finally, our calculations show the well-known trend that the LDA functional underestimates the lattice parameters, while the GGA functional overestimates them.

3.2. Electronic Properties

Figure 2 shows the calculated density of states (DOS) for the three systems studied, where spin polarization effects have been considered. For comparison the total DOS found for the GGA and on-site hybrid functionals are depicted (upper panel). The obtained DOS show almost the same features independent of the functional used, with the exception of the low conduction bands for the MoSSe system where some discrepancies for the amplitude were obtained. These results could be related with the fact that the Mo 4*d* states fully hybridizate with the chalcogen p states, instead to be highly localized,[21] as has been also noted in an early report for bulk MoS_2.[22] On the other hand, it can be seen that the calculated DOS are symmetric for the spin-up and spin-down polarization. This effect is the expected one because we have an isoelectronic substitution for the chalcogen XY (X, Y = S, Se, Te), implying that no magnetic order is expected from our calculations. The main contribution to the VBM and conduction band minimum (CBM) originated from the hybridization of the Mo 4*d* orbitals with the chalcogen p-states, resulting in good agreement with previous works.[19,20] For the partial DOS (lower panel), we observe that the lighter anion has a more significant contribution to the energies at the VBM, i.e., yellow lines for S in **Figure 3**d,f, and purple lines for Se in Figure 3e. On the other hand, at the CBM, the critical contribution of the chalcogen comes from the heavy chalcogen ion.

Figure 3 shows the computed electronic band structure for the three systems studied in this work, where circles depict the atomic orbital contributions to the electronic band structure. The larger circles correspond to a higher charge within the atomic sphere, qualitatively showing those orbitals that constitute each electronic band.[9]

As we have commented above, from the calculated partial density of states (PDOS), the VBM has mainly the character of the Mo 4*d* states; to further understand the energy range of

© 2021 Wiley-VCH GmbH

15213951, 2022, 1, Downloaded from https://onlinelibrary.wiley.com/doi/10.1002/pssb.202100248 by Academia Sinica, Wiley Online Library on [26/03/2025]. See the Terms and Conditions (https://onlinelibrary.wiley.com/terms-and-conditions) on Wiley Online Library for rules of use; OA articles are governed by the applicable Creative Commons License

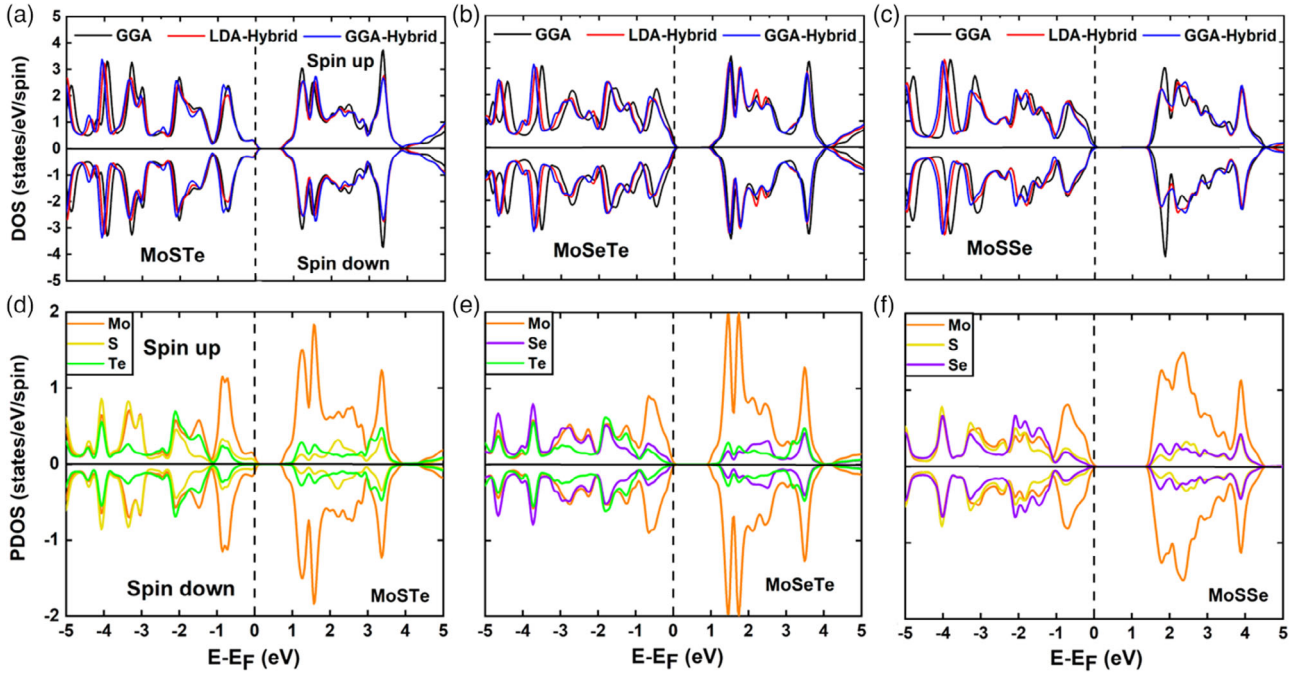

Figure 2. Upper panel: Total density of states for: a) MoSTe, b) MoSeTe, c) MoSSe monolayers, comparison of the GGA and on-hybrid calculations. Lower panel: PDOS for: d) MoSTe, e) MoSeTe, and f) MoSSe monolayers.

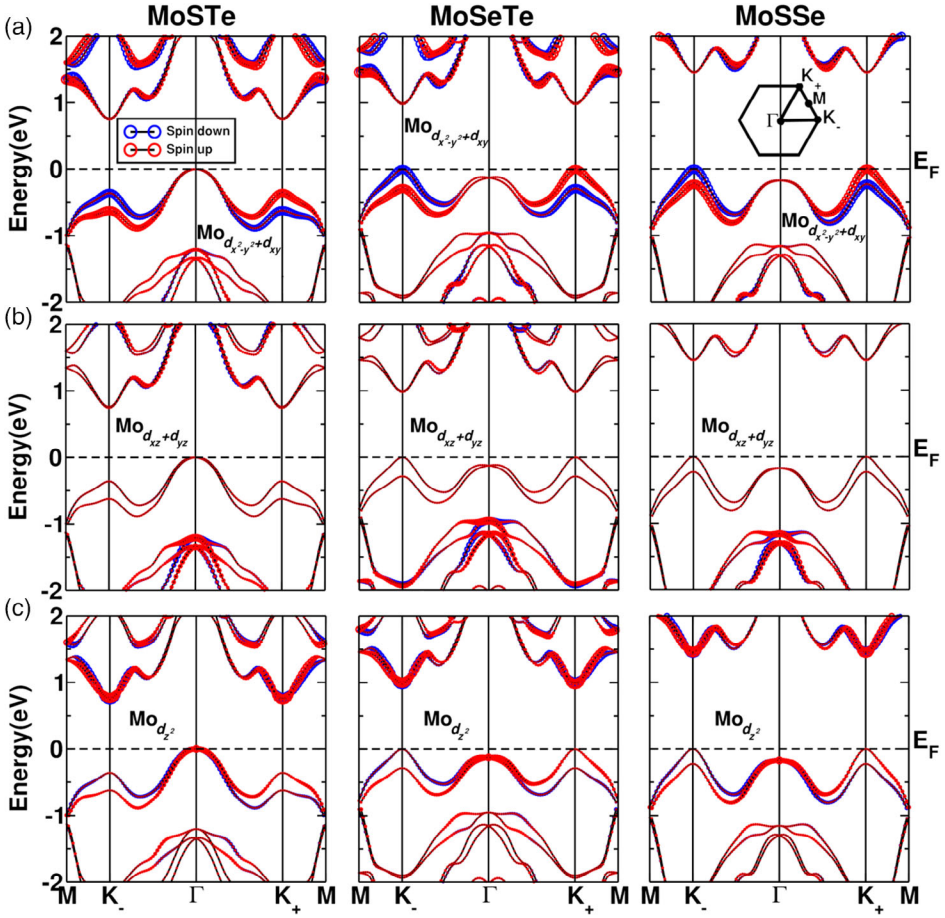

Figure 3. Calculated Mo 4*d* atomic orbital contributions to the electronic band structure for the MoSTe, MoSeTe, and MoSSe Janus monolayer. The upper panel shows Mo $4(d_{(x^2-y^2)} + d_{xy})$, the middle panel shows Mo $4(d_{xz} + d_{yz})$, and the lower panel shows the Mo $4d_z^2$orbital.

© 2021 Wiley-VCH GmbH

15213951, 2022, 1, Downloaded from https://onlinelibrary.wiley.com/doi/10.1002/pssb.202100248 by Academia Sinica, Wiley Online Library on [26/03/2025]. See the Terms and Conditions (https://onlinelibrary.wiley.com/terms-and-conditions) on Wiley Online Library for rules of use; OA articles are governed by the applicable Creative Commons License

Table 2. Calculated energy bandgap (E_g) for Mo-XY (X, Y = S, Se, Te) monolayers.

	MoSTe	MoSeTe	MoSSe
E_g [eV]	0.74[a)]	0.98[a)]	1.41[a)]
	0.71[b)]	1.10[b)]	1.54[b)]
	0.70[c)]	0.98[c)]	1.42[c)]
	1.59[d)]	1.59[d)]	1.95[d)]
	1.99[e)]	1.84[e)]	2.33[e)]

[a)]GGA; [b)]GGA-hybrid; [c)]LDA-hybrid; [d)]HSE06,[5] [e)]G_0W_0.[5]

the contribution of each orbital, we plotted the Mo $4(d_{(x^2-y^2)} + d_{xy})$, Mo $4(d_{xz} + d_{yz})$, and $4d_z{}^2$ orbitals in Figure 3a–c, respectively. The red circles show the spin-up population, while the blue circles show the spin-down population.

For the valley along with the K_- –Γ–K_+ trajectory, the main contribution to the valence band energy range comes from the Mo $4(d_{(x^2-y^2)} + d_{xy})$ orbitals. As discussed by Lu et al.,[4] similar orbital contributions to the bands at the upper VB as well in the lower CB are obtained. In contrast, the Mo $4(d_{xz} + d_{yz})$ states show an important contribution at Γ point in the low energies of the VB and high energies of the CB. Finally, the Mo $4d_z{}^2$ states are essential in the VBM at Γ, indicating that the splitting of these states is responsible for the Rashba effect. **Table 2** shows the computed bandgap value of the three systems using (a) GGA, (b) GGA-hybrid, and (c) LDA-hybrid which are also compared with HSE0(d) and G_0W_0(e) approaches reported in the computational database of 2D materials.[5,16,17] It can be noticed that MoSeTe and MoSSe monolayers are direct bandgap systems at the K point with values around 0.98, 1.1, and 0.98 and 1.41, 1.54, and 1.42 eV, respectively. On the other hand, the MoSTe Janus monolayer has an indirect bandgap, where the obtained transition is from the Γ–K points, and a calculated value of 0.74, 0.71, and 0.70 eV. Although we found that our calculated values differ from those calculated using the HSE06 functional, or the quasiparticle G_0W_0 approach reported by Riis-Jensen,[5] it is also found that our values are consistent with previous works.[3,4,20,21,23]

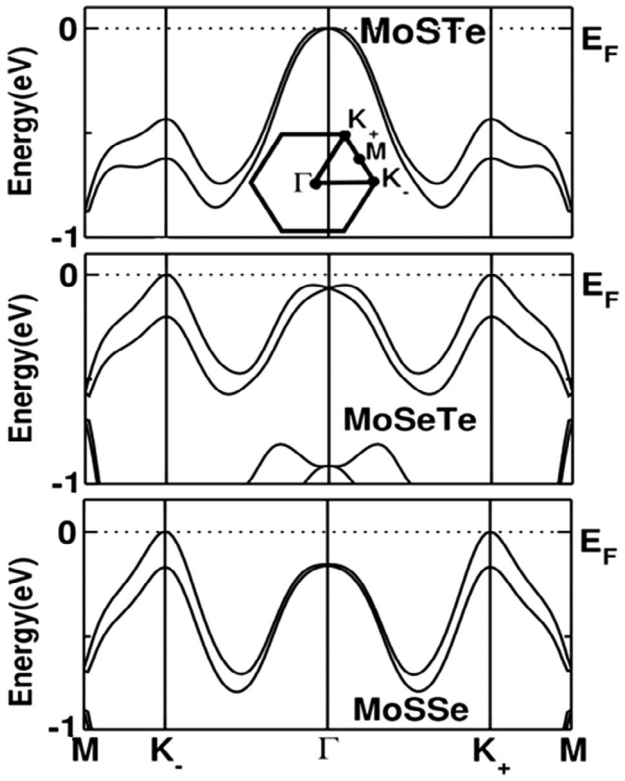

Figure 4. Calculated electronic band structure for MoSTe, MoSeTe, and MoSSe at the upper valence bands range.

Figure 4 depicts the calculated electronic band structure for the studied Janus monolayers at the upper VB energies range. We can observe that, at Γ point, the Rashba splitting is obtained, while at K_- and K_+ points, the Zeeman energy splitting is also found. Figure 4b shows that the Zeeman effect is more noticeable for the MoSeTe Janus monolayer, in good agreement with previous reports.[3,4] Finally, our findings revealed that the Rasha effect is present in the three proposed Janus monolayers; however, we believe that MoSSe and MoSeTe monolayer systems represent unique properties because it is possible to combine the Rashba effect along with the optical valley selection rules to develop novel spintronic devices.

4. Conclusions

In summary, we have found that MoXY (X, Y = S, Se, Te) Janus monolayers present a spin polarization near the high symmetry Γ, K_-, and K_+ points of the valence band which are highly modulated by the Mo 4*d* orbitals. Among the three studied systems, MoSeTe and MoSSe Janus monolayers present spin–valley polarization, Rashba spin-splitting, and a direct bandgap, representing an interesting atomically thin material that can be exploited in different applications such as spintronics, spin-orbitronics, and nanoelectronics. Our calculations were done using the GGA and on-site hybrid functionals, as we have found both functionals show similar results for the electronic properties of the studied systems.

Acknowledgements

M.A.H.V. thanks CONACyT-Mexico for his Ph.D. scholarship. D.O. acknowledges SEP-CONACyT-Mexico for the partial financial support through grant FIDSC2018/211. The computational resources from LANCAD and CONACyT in the Supercomputer Hybrid Cluster "Xiuhcoatl" at General Coordination of Information and Communications Technologies (CGSTIC) of CINVESTAV are also acknowledged.

Conflict of Interest

The authors declare no conflict of interest.

Data Availability Statement

Research data are not shared.

© 2021 Wiley-VCH GmbH

15213951, 2022, 1, Downloaded from https://onlinelibrary.wiley.com/doi/10.1002/pssb.202100248 by Academia Sinica, Wiley Online Library on [26/03/2025]. See the Terms and Conditions (https://onlinelibrary.wiley.com/terms-and-conditions) on Wiley Online Library for rules of use; OA articles are governed by the applicable Creative Commons License

Keywords

ab initio calculations, Janus monolayers, Rashba effect, Zeeman spin-splitting

Received: May 31, 2021
Revised: October 19, 2021
Published online: November 17, 2021

[1] Y. K. Luo, J. Xu, T. Zhu, G. Wu, E. J. McCormick, W. Zhan, M. R. Roland, R. K. Kawakami, *Nano Lett.* **2017**, *17*, 3877.
[2] K. S. Thygesen, *2D Mater.* **2017**, *4*, 022004.
[3] Y. C. Cheng, Z. Y. Zhu, M. Tahir, U. Schwingenschlögl, *Europhys. Lett.* **2013**, *102*, 57001.
[4] A. Y. Lu, H. Zhu, J. Xiao, C. P. Chuu, Y. Han, M. H. Chiu, C. C. Cheng, C. W. Yang, K. H. Wei, Y. Yang, Y. Wang, D. Sokaras, D. Nordlund, P. Yang, D. A. Muller, M. Y. Chou, X. Zhang, L. J. Li, *Nat. Nanotechnol.* **2017**, *12*, 774.
[5] A. C. Riis-Jensen, T. Deilmann, T. Olsen, K. S. Thygesen, *ACS Nano* **2019**, *13*, 13354.
[6] J. Gusakova, X. Wang, L. L. Shiau, A. Krivosheeva, V. Shaposhnikov, V. Borisenko, V. Gusakov, B. K. Tay, *Phys. Status Solidi A* **2017**, *214*, 1700218.
[7] Q. F. Yao, J. Cai, W. Y. Tong, S. J. Gong, J. Q. Wang, X. Wan, C. G. Duan, J. H. Chu, *Phys. Rev. B* **2017**, *95*, 165401.
[8] A. Manchon, H. C. Koo, J. Nitta, S. M. Frolov, R. A. Duine, *Nat. Mater.* **2015**, *14*, 871.
[9] P. Blaha, K. Schwarz, J. Luitz, *WIEN97*, K. Schwarz, Techn. Univ. Wien, Vienna **1999**. [Improved and updated Unix version of the original copyrighted WIEN code, which was published by P. Blaha, K. Schwarz, P. Sorantin, S. B. Trickey, *Comput. Phys. Commun.* **1990**, *59*, 339].
[10] a) J. P. Perdew, Y. Wang, *Phys. Rev. B* **1992**, *46*, 12947; b) J. P. Perdew, K. Burke, M. Ernzerhof, *Phys. Rev. Lett.* **1996**, *77*, 3865.
[11] F. Tran, P. Blaha, K. Schwarz, *Phys. Rev. B* **2006**, *74*, 155108.
[12] F. Tran, J. Doumont, L. Kalantari, A. W. Hurn, M. A. L. Marques, P. Blaha, *J. Appl. Phys.* **2019**, *126*, 110902.
[13] P. Novak, J. Kunes, L. Chaput, W. E. Pickett, *Phys. Status Solidi B* **2006**, *243*, 563.
[14] H. J. Monkhorst, J. D. Pack, *Phys. Rev. B* **1976**, *13* 5188.
[15] F. D. Murnaghan, *Proc. Natl. Acad. Sci. USA* **1994**, *30*, 224.
[16] S. Haastrup, M. Strange, M. Pandey, T. Deilmann, P. S. Schmidt, N. F. Hinsche, M. N. Gjerding, D. Torelli, P. A. Larsen, A. C. Riss-Jensen, *2D Mater.* **2018**, *5*, 042002.
[17] M. N. Gjerding, A. Taghizadeh, A. Rasmussen, S. Ali, F. Bertoldo, T. Deilmann, N. R. Knøsgaard, M. Kruse, A. H. Larsen, S. Manti, T. G. Pedersen, U. Petralanda, T. Skovhus, M. K. Svendsen, J. J. Mortensen, T. Olsen, K. S. Thygesen, *2D Mater.* **2021**, *8*, 044002.
[18] J. Wang, H. Shu, X. Chen, *Phys. Chem. Chem. Phys.* **2018**, *20*, 18571.
[19] W.-Y. Yin, B. Wen, G.-Z. Nie, X.-L. Wei, L.-M. Liu, *J. Mater. Chem. C* **2018**, *6*, 1693.
[20] X. Yang, D. Singh, R. Ahuja, *J. Mater. Chem. C* **2019**, *7*, 12312.
[21] It will be also possible to use the DFT+U approach, however, this method is for studying the high-correlated 3d, 4f electrons, and our studied systems contain Mo with 4d electrons. There it is found that at the upper valence bands, these electrons hybridize with the chalcogen p electrons, as we have commented in Figure 3. [See also M. Wu, X. Yao, Y. Hao, H. Dong, Y. Cheng, H. Liu, F. Lu, W. Wang, K. Cho, W.-H. Wang, *Phys. Lett. A* **2018**, *382*, 111]. On the other hand, there is few information for the U parameter in Mo-X2 systems. [See for example C. Ataca, H. Şahin, S. Ciraci, *J. Phys. Chem. C* **2012**, *116*, 8983].
[22] D. Li, G. M. Bancroft, M. Kasrai, M. E. Fleet, X. H. Feng, K. H. Tan, *Phys. Chem. Miner.* **1995**, *22*, 123.
[23] J. Zhang, S. Jia, I. Kholmanov, L. Dong, D. Er, W. Chen, H. Guo, Z. Jin, V. B. Shenoy, L. Shi, L. Lou, *ACS Nano* **2017**, *11*, 8192.

© 2021 Wiley-VCH GmbH

15213951, 2022, 1, Downloaded from https://onlinelibrary.wiley.com/doi/10.1002/pssb.202100248 by Academia Sinica, Wiley Online Library on [26/03/2025]. See the Terms and Conditions (https://onlinelibrary.wiley.com/terms-and-conditions) on Wiley Online Library for rules of use; OA articles are governed by the applicable Creative Commons License